



Resonantlike Synchronization and Bursting in a Model of Pulse-Coupled Neurons with Active Dendrites

PAUL C. BRESSLOFF

*Nonlinear and Complex Systems Group, Department of Mathematical Sciences, Loughborough University,
Loughborough, Leicestershire, LE11 3TU, UK*

Received June 12, 1998; Revised September 8, 1998; Accepted October 1, 1998

Action Editor: G. Bard Ermentrout

Abstract. We analyze the dynamical effects of active, linearized dendritic membranes on the synchronization properties of neuronal interactions. We show that a pair of pulse-coupled integrate-and-fire neurons interacting via active dendritic cables can exhibit resonantlike synchronization when the frequency of the oscillators is approximately matched to the resonant frequency of the membrane impedance. For weak coupling the neurons are phase-locked with constant interspike intervals whereas for strong coupling periodic bursting patterns are observed. This bursting behavior is reflected by the occurrence of a Hopf bifurcation in the firing rates of a corresponding rate-coded model.

Keywords: integrate-and-fire, active membranes, dendrites, bursting

1. Introduction

The passive membrane properties of a neuron's dendritic tree result in a diffusive spread of current through the system that causes changes in the membrane potential along the tree. Such a diffusive process is commonly described mathematically in terms of a second-order linear partial differential equation known as the cable equation. Rall (1962) showed how such an equation can represent an entire dendritic tree in terms of an equivalent one-dimensional cable for certain restricted geometries. In a later development he pioneered the idea of modeling a dendritic tree as a graph of connected electrical compartments (Rall, 1964). Compartmental modeling represents a finite-difference approximation of a linear cable equation in which the dendritic system is divided into sufficiently small regions such that spatial variations of the electrical and physical properties within a region are negligible. The partial differential equations of cable theory then simplify to a system of first-order ordinary

differential equations. In practice, a combination of matrix algebra and numerical methods are often used to solve for realistic neuronal geometries (Perkel et al., 1981; Segev et al., 1989).

Recent experiments suggest that the representation of dendrites in terms of purely passive membranes is an oversimplification, since there exists a variety of active, voltage-dependent ionic channels distributed along the dendritic tree. For example, intradendritic recordings in both hippocampal pyramidal cells (Wong et al., 1979; Poolos and Kocsis, 1990; Johnston et al., 1996) and neocortical pyramidal cells (Amitai et al., 1993; Stuart and Sakmann, 1994; Svoboda et al., 1997) have demonstrated that a complex combination of fast and slow dendritic spikes can be induced by current injection. It has been suggested that such active processes could be important for information processing, with local computations carried out on clusters of synapses (Shepherd and Brayton, 1987; Mel, 1994). In general, the dependence of active channel conductances on voltage and time involves a complicated nonlinear

process that is not described by linear cable theory, although such features can be handled numerically using a compartmental approach (Mainen and Sejnowski, 1996; Jaeger et al., 1997; Jackson and Cauller, 1997). Further complications arise due to the fact that many excitatory inputs to cortical pyramidal cells synapse on tiny protrusions known as dendritic spines. In order to take proper account of such small structures, the standard cable equation needs to be replaced by a nonlinear electro-diffusion model that can handle rapid changes in ionic concentration (Qian and Sejnowski, 1989).

Nevertheless, linear cable theory has proved a very useful theoretical tool in understanding certain aspects of active dendritic processing. For example, neuronal models have been developed that combine active properties in spine head membranes with the passive properties of the dendritic shaft to which the spines are attached (Koch and Poggio, 1983; Coss and Perkel, 1985; Miller et al., 1985). Computations have established that the excitable spine head can nonlinearly amplify synaptic inputs, leading to an increased amount of current delivered to the dendrite and thus enhancing the synapse's efficacy. Such processes have been linked with Hebbian learning mechanisms (Zador et al., 1990). Furthermore, for relatively small deviations of the membrane potential, a linearization of the channel kinetics is also appropriate. The resulting continuum cable model of the dendrites has a membrane impedance that displays resonantlike behavior due to the additional presence of inductances (Koch, 1984). It is known that such resonant behavior subserves specific neuronal functions. For example, hair cells of a vertebrate cochlear exhibit their maximal sensitivity at some nonzero frequency that depends on their location along the cochlear (Crawford and Fettiplace, 1981). Moreover, rod photoreceptors of lower vertebrates have a receptive field that increases with the temporal frequency of the stimulus (Torre and Owen, 1983).

Diffusion along the dendritic tree generates an effective spatiotemporal distribution of delays as expressed by the associated Green's function of the cable equation. The Green's function determines the linear response to an instantaneous injection of unit current at a given point on the tree. Various mathematical methods have been developed to calculate the Green's function for the cable equation in one dimension (Tuckwell, 1988; Rall, 1989), in the presence of shunting (Poggio and Torre, 1977), and for nontrivial geometries (Abbott et al., 1991). Previous work by

the author has demonstrated that delays arising from passive dendritic interactions can have a significant influence on the dynamical behavior of coupled neural systems (Bressloff, 1994; Bressloff and de Souza, 1998). See in particular the review by Bressloff and Coombes (1997). Passive dendritic interactions have also been studied by Crook et al. (1997, 1998) and Bressloff and Coombes (1997) in the case of weakly coupled phase oscillators.

In this article we use linear cable theory to study the effects of delays arising from passive and (linearized) active dendrites on the synchronization properties of neuronal interactions. In order to proceed analytically, we shall develop our discussion in terms of an integrate-and-fire model of pulse-coupled neural oscillators (see the reviews in Tuckwell, 1988; Gerstner, 1995). This class of model can be derived systematically by a reduction procedure from the Hodgkin-Huxley equations (Abbott and Kepler, 1991; Kistler et al., 1997). We shall follow van Vreeswijk et al. (1994) in their study of the synchronization properties of synaptic (α -function) delays and take as our starting point a pair of identical integrate-and-fire neurons with dendritic interactions that are mediated by diffusion along a uniform, semi-infinite cable. The stability of phase-locked solutions, in which both neurons fire at the same constant frequency, is determined as a function of the dendritic location of synapses and the collective frequency of oscillations. In particular, we show how dendrites with active, linearized membranes induce a form of resonantlike synchronization. That is, if the resonant frequency of the cable approximately matches the frequency of the oscillators, then there is a strongly enhanced (reduced) tendency to synchronize for weak excitatory (inhibitory) coupling. It is then shown how active dendrites can destabilize a pair of phase-locked neurons in the strong coupling regime leading to a state with time-periodic variations in the interspike intervals—that is, bursting patterns. The bursting behavior is reinterpreted in terms of a corresponding analog or rate-coded version of the IF model, which is shown to undergo a Hopf bifurcation to a state with synchronous (anti-synchronous) periodic firing rates in the case of excitatory (inhibitory) coupling. The occurrence of bursting is particularly interesting given the recent numerical study of compartmental models of neocortical neurons that demonstrated how active dendrites can strongly influence the bursting properties of neurons (Mainen and Sejnowski, 1996).

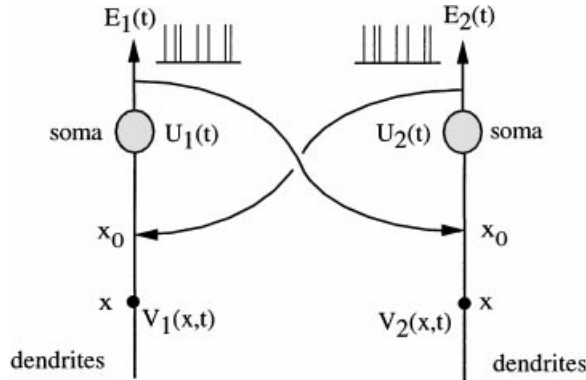


Figure 1. Basic interaction picture.

2. Phase-Locking of IF Oscillators with Passive Dendrites

Consider a pair of identical integrate-and-fire (IF) neural oscillators coupled together via axo-dendritic synapses as shown in Fig. 1. We assume that the coupling is symmetric. Each oscillator consists of a soma or cell body where spike generation occurs together with a dendritic tree modeled as a uniform semi-infinite cable. Let $U_i(t)$ denote the somatic potential of the i th neuron at time t and take $I_i^{\text{syn}}(t)$ to be the corresponding input current flowing into the soma from the dendritic cable, $i = 1, 2$. Suppose that the variables $U_i(t)$ evolve according to the set of equations

$$\frac{dU_i(t)}{dt} = -\frac{U_i(t)}{\tau_s} + I + I_i^{\text{syn}}(t) \quad (1)$$

supplemented by the condition that whenever $U_i = 1$ it is immediately reset to $U_i = 0$. Here τ_s is the membrane time constant of the soma and I is a time-independent external input.

The membrane potential at the point x , $0 \leq x < \infty$ on the dendritic cable of the i th neuron is denoted by $V_i(x, t)$. Let $P(x)$ represent the distribution of axon collaterals from one neuron making synapses on the dendritic cable of the other neuron, with $P(x) \geq 0$ and $\int_0^\infty P(x) dx = 1$. For the moment we shall assume that the membrane properties of each cable are purely passive. (Active linearized membranes will be considered in Section 3.) Standard cable theory then allows us to write down the following equation for $V_i(x, t)$ (Rall, 1964)

$$\frac{\partial V_i(x, t)}{\partial t} = -\frac{V_i(x, t)}{\tau_d} + D \frac{\partial^2 V_i(x, t)}{\partial x^2} + \epsilon P(x) E_j(t) \quad (2)$$

for $j \neq i$ where τ_d is the membrane time constant and D is the diffusivity of the cable. Electronic distance along the cable is measured in terms of the membrane space constant $\sigma = \sqrt{\tau_d D}$. In Eq. (2), ϵ determines the strength of interactions, with $\epsilon > 0$ ($\epsilon < 0$) corresponding to excitatory (inhibitory) coupling, and $E_j(t)$ denotes the output spike train from the j th oscillator. If we neglect the finite shape of a pulse arising from the effects of synaptic and axonal delays, which are discussed elsewhere (van Vreeswijk et al., 1994; Bressloff and Coombes, 1998a, 1998b), then $E_j(t)$ may be represented as a sequence of unit impulses or Dirac delta-functions $E_j(t) = \sum_{m=-\infty}^{\infty} \delta(t - T_j^m)$, where the T_j^m are the firing times of the j th neuron. At the end of the dendritic cable adjoining the soma we impose the homogeneous boundary condition $\partial V_i(x, t)/\partial x|_{x=0} = 0$. Note that this assumes that the feedback current from the soma to the dendritic cable can be neglected (Bressloff, 1995). Finally, we set $I_i^{\text{syn}}(t) = \kappa [V_i(0, t) - U_i(t)]$ where κ is a conductance (in appropriate units).

Equation (2) can be solved in terms of the Green's function $G(x, t)$ of the given cable equation (Tuckwell, 1988):

$$V_i(0, t) = \epsilon \int_0^\infty J(t') E_j(t - t') dt', \quad (3)$$

where $J(t) = \int_0^\infty P(x) G(x, t) dx$ and

$$G(x, t) = \frac{e^{-t/\tau_d}}{\sqrt{\pi D t}} e^{-x^2/4Dt} \Theta(t) \quad (4)$$

with $\Theta(t) = 1$ if $t \geq 0$ and zero otherwise. The Green's function $G(x, t)$ determines the membrane potential response at the end of the cable due to an instantaneous injection of unit current at point x at time t . For concreteness, we shall assume that the synapses are located at a single point x_0 on the cable so that $J(t) = G(x_0, t)$. If we now substitute Eq. (3) into (1) and fix the units of time by setting $\tau_s^{-1} + \kappa = 1$, then Eq. (1) reduces to

$$\frac{dU_i(t)}{dt} = -U_i(t) + I + X_i(t) \quad (5)$$

with

$$X_i(t) = \epsilon \sum_{m=-\infty}^{\infty} J(t - T_j^m). \quad (6)$$

A factor of κ has been absorbed into the coupling parameter ϵ . Equations (5) and (6) are identical in form to the system of equations considered by van Vreeswijk

et al. (1994) for synaptic delays, and we shall follow their method of analysis. It will be assumed that $I > 1$ so that in the absence of any coupling ($\epsilon = 0$) the neurons fire at a constant rate $T_0 = \ln[I/(I - 1)]$

We first look for phase-locked solutions of Eqs. (5) and (6) in which the firing times take the form $T_j^m = (m - \phi_j)T$ for all integer m and $j = 1, 2$, where T is a self-consistent collective period and $0 \leq \phi_j < 1$. Integrating Eq. (5) between two successive firing events leads to a pair of equations for T and $\phi = \phi_2 - \phi_1$:

$$1 = I(1 - e^{-T}) + \epsilon K_T(\pm\phi), \quad (7)$$

where

$$K_T(\phi) = e^{-T} \int_0^T e^t \sum_{m=-\infty}^{\infty} J([\phi + m]T + t) dt. \quad (8)$$

Since $K_T(\phi)$ is a periodic function of ϕ , it can be expressed in terms of a Fourier series. That is,

$$K_T(\phi) = \frac{1 - e^{-T}}{T} \sum_{m=-\infty}^{\infty} h(2\pi m/T) e^{2\pi i m \phi}, \quad (9)$$

where

$$h(\omega) = \frac{\tilde{G}(x_0, \omega)}{1 + i\omega} \quad (10)$$

and

$$\tilde{G}(x, \omega) = \frac{1}{D\gamma(\omega)} e^{-\gamma(\omega)x} \quad (11)$$

is the transfer function (Fourier transformed Green's function) for the given dendritic cable with

$$\gamma(\omega)^2 = \frac{1 + i\omega\tau_d}{D\tau_d}. \quad (12)$$

Note that $\gamma(\omega)$ in Eq. (12) is related to the membrane impedance of the dendritic cable (see Section 3). For purely passive membranes, the impedance is a function of capacitances and resistances so that the cable acts as a low-pass filter. That is, both $|\gamma(\omega)|$ and $|\tilde{G}(x, \omega)|$ (for fixed x) attain their maximum value at $\omega_{\max} = 0$. On the other hand, active dendrites can be modeled in terms of an impedance that also depends on inductances. The cable now acts as a band-pass filter with $\omega_{\max} \neq 0$. The consequences of such a resonance will be explored in later sections. The calculation of $h(\omega)$ for the resonant case is presented in Appendix A.

The pair of equations in (7) determines both the relative phase ϕ and the collective period T of oscillations.

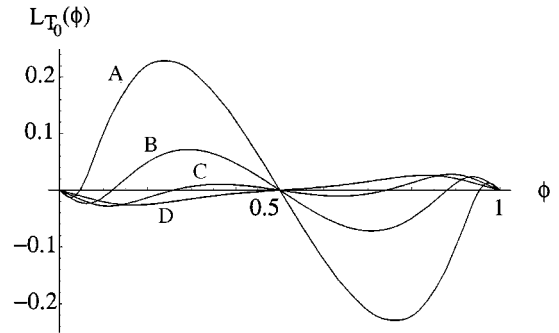


Figure 2. Odd phase interaction function $L_{T_0}(\phi)$ for a range of values of dendritic distance x_0 with $T_0 = \pi$, $\sigma = 1$, $\tau_d = 1$. The functions are determined from a truncated version of the Fourier series (9) with $|m| \leq 10$. A: $x_0 = 1.0$, B: $x_0 = 1.5$, C: $x_0 = 2.0$, D: $x_0 = 2.5$.

Assume, for the moment, that the neurons are weakly coupled such that $\epsilon \ll 1$. Then $T \approx T_0$ and the allowed solutions for ϕ are given by the zeroes of $L_{T_0}(\phi)$ where $L_T(\phi) = K_T(\phi) - K_T(-\phi)$. The underlying symmetry of the system guarantees the existence of the *in-phase* or synchronous solution $\phi = 0$ and the *antiphase* or antisynchronous solution $\phi = 1/2$. It is also possible for asynchronous solutions to occur in certain parameter regimes. This is illustrated in Fig. 2, where we plot the odd function $L_{T_0}(\phi)$ for a range of dendritic locations x_0 and σ , $\tau_d = 1$. We approximate the interaction function $K_{T_0}(\phi)$ by truncating the Fourier series (9) such that $|m| \leq M$. We can estimate a reasonable choice for M by noting that $h(\omega) \sim \omega^{-3/2} e^{-\sqrt{\omega/2}x_0}$ for large ω and hence M should satisfy the condition $(\pi M/T_0)^{-3/2} e^{-\sqrt{\pi M/T_0}x_0} \ll 1$. For fixed coupling ϵ and large x_0/σ one finds that the in-phase and antiphase solutions are the only phase-locked solutions. However, as x_0/σ is decreased, a critical value is reached where there is a bifurcation of the antiphase solution leading to the creation of two partially synchronized states θ and $1 - \theta$, with $0 < \theta < 1/2$ and $\theta \rightarrow 0$ as $x_0/\sigma \rightarrow 0$. Analogous results are found for synaptic delays (van Vreeswijk et al., 1994).

In the weak coupling regime a phase-locked solution ϕ will be stable if and only if (van Vreeswijk et al., 1994)

$$\epsilon \frac{dL_{T_0}(\phi)}{d\phi} > 0. \quad (13)$$

Using the Fourier representation (9), we numerically determine the stability regions in parameter space for excitatory coupling ($\epsilon > 0$). The results are shown in Fig. 5A. We have approximated the derivative

of $K_{T_0}(\phi)$ by truncating the Fourier series such that $|m| \leq M$ with M satisfying the condition $e^{-\sqrt{\pi M/T_0}x_0}/\sqrt{\pi M/T_0} \ll 1$. It is convenient for computational purposes to ensure that M is not too large. Therefore, we restrict our analysis to the domain $x_0 \geq 1$ and $T_0 \leq 2\pi$ and take $M = 100$. It is clear from Fig. 5A that the synchronous state is unstable when $x_0 = 1$, and that as x_0 increases one obtains alternating bands of stability and instability. (These regions of stability/instability are reversed for inhibitory coupling.) We conclude that the dendritic location of a synapse x_0 can potentially influence whether neuronal interactions are synchronizing or desynchronizing (see also Crook et al., 1997, 1998; Bressloff and Coombes, 1997).

3. Resonantlike Synchronization for Active Dendrites

In our analysis so far, we have assumed that the cell membranes of the dendrites are purely passive. That is, they can be modeled in terms of resistances in parallel with capacitances, which in the continuum limit leads to the cable Eq. (2). As discussed in the introduction, recent experiments suggest that there exist a variety of active, voltage-dependent ionic channels distributed along the dendritic tree. In general, the active channel conductances depend nonlinearly on voltage and time. However, for relatively small deviations of the membrane potential from the resting potential of the cell, one can linearize the channel kinetics. The cell membrane can then be analyzed in terms of a linear electrical system consisting of resistors, capacitors, and inductors (Koch, 1984). The presence of inductance means that the neuron behaves like a band-pass filter, in the sense that its membrane impedance has a maximum modulus at a nonzero (resonant) frequency; purely passive membranes act as low-pass filters.

Almost all of the analytical work to date on active dendrites has been restricted to the case of single neuron properties. Here we are interested in exploring the effects of linearized active dendritic membranes on the dynamical behavior of networks of neurons, more specifically, how the band-pass nature of the dendrites alters the synchronizing properties of neuronal interactions. It is a relatively simple matter to extend our previous analysis to incorporate active dendrites, since one only needs to modify the form factor $\gamma(\omega)$ appearing in the transfer function (11). We follow closely the treatment of Koch (1984). First, we represent a linear one-dimensional cable as a semi-infinite

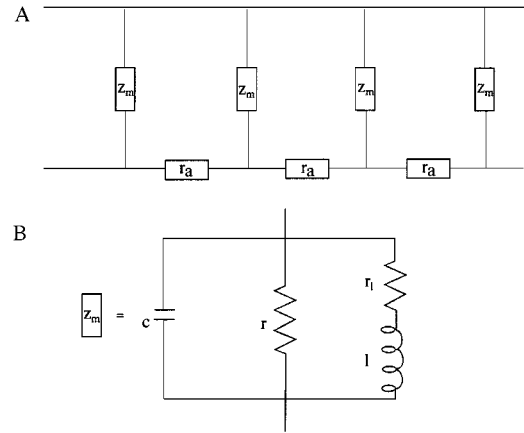


Figure 3. A: Ladder representation of a one-dimensional cable with frequency-dependent membrane impedance $z_m(\omega)$ and longitudinal resistance r_a . B: Electric circuit of a linearized active membrane.

ladder network as shown in Fig. 3A. Let $z_m(\omega)$ denote the frequency-dependent membrane impedance and r_a the longitudinal resistance of a unit length of cable. In the continuum limit, one obtains a cable equation whose corresponding transfer function satisfies Eq. (11) with

$$\gamma(\omega)^2 = \frac{r_a}{z_m(\omega)}. \quad (14)$$

For a purely passive membrane,

$$z_m(\omega) = \frac{r}{1 + i\omega\tau_d}, \quad (15)$$

where $\tau_d = rc$, and r, c are the membrane leakage resistance and capacitance for a cable of unit surface area. Comparison of Eqs. (14) and (15) with Eq. (12) shows that $D\tau_d = r/r_a$.

A simple model of an active linearized membrane is an electrical circuit consisting of a passive component in parallel with an inductive branch containing an inductance l in series with a resistance r_l (Fig. 3B). At a phenomenological level this represents the electrical behavior of a specific type of active channel for small variations in the membrane potential (Koch, 1984). For such a circuit,

$$z_m(\omega) = \frac{r(r_l + i\omega l)}{r + r_l - \omega^2 l\tau_d + i\omega(l + r_l\tau_d)}. \quad (16)$$

(In the limit $r_l \rightarrow \infty$ one recovers Eq. (15)). Substituting Eqs. (14) and (16) into Eqs. (10) and (11), and

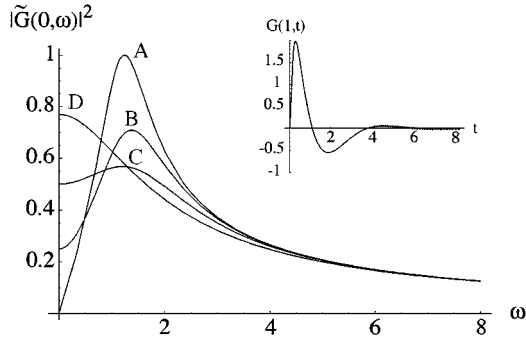


Figure 4. Modulus of transfer function $|\tilde{G}(0, \omega)|^2$ (in units of $1/(D^2 r_a)$) as a function of frequency ω (in units of τ_d^{-1}) for various values of inductive resistance r_l . Here $r = 0.3 \Omega\text{m}^2$, $c = 0.01 \text{Fm}^{-2}$ and $l = 6 \times 10^{-4} \text{Hm}^2$. A transition from band-pass to low-pass filtering can be seen as r_l increases. A: $r_l = 0$, B: $r_l = 0.1$, C: $r_l = 0.3$, D: $r_l = 1.0 \Omega\text{m}^2$. Inset: Plot of Green's function $G(x, t)$ at $x = 1$ as a function of time t (in units of τ_d) for $r_l = 0.1 \Omega\text{m}^2$.

taking real and imaginary parts then allows us to determine the phase interaction function $K_T(\phi)$, Eq. (9), in the presence of active dendrites (see Appendix A).

It is well known that the introduction of an inductance into an electrical circuit can lead to resonantlike behavior in which the impedance $|z_m(\omega)|$ goes through a maximum at some nonzero resonant frequency ω_{\max} . For the circuit of Fig. 3B there exists a maximum at

$$\omega_{\max} = [-(r_l/l)^2 + ((r_l/l)^4 - E)^{1/2}]^{1/2}, \quad (17)$$

provided that $E \equiv (Br_l^2 - l^2C)/(Al^2) < 0$ (Koch, 1984). The constants A, B, C are defined below Eq. (A7)

in Appendix A. In the case of an ideal resonant circuit ($r_l = 0$), $\omega_{\max} = 1/\sqrt{lc}$. As r_l is increased from zero, ω_{\max} first increases and then decreases until a critical value of r_l is reached beyond which there is no maximum impedance. That is, the system acts as a low-pass filter rather than a band-pass filter. It can also be shown that if the impedance $z_m(\omega)$ has band-pass characteristics then so does the transfer function $\tilde{G}(x, \omega)$ of Eq. (11)—that is,

$$|\tilde{G}(x, \omega)|^2 = \frac{1}{D^2 r_a} |z_m(\omega)| e^{-2\text{Re}(\gamma(\omega))}$$

has a maximum at ω_{\max} , where $a(\omega)$ denotes the real part of $\gamma(\omega)$. The amplitude $|\tilde{G}(0, \omega)|$ is plotted in Fig. 4 as a function of ω and various inductive resistances r_l . The biologically plausible values of the membrane parameters are taken from (Koch, 1984): $r = 0.3 \Omega\text{m}^2$, $c = 0.01 \text{Fm}^{-2}$, $r_a = 2.8 \times 10^6 \Omega$, $r_l = 0.1 - 1 \Omega\text{m}^2$, $l = 6 \times 10^{-4} \text{Hm}^2$. For these particular values, the membrane time constant $\tau_d = 3 \text{ms}$ and the membrane space constant $\sigma = \sqrt{D\tau_d} \approx 300 \mu\text{m}$. The band-pass nature of the transfer function is reflected in the behavior of the real-time Green's function $G(x, t)$, which develops an oscillatory component (see inset of Fig. 4). We now investigate how the presence of a resonance in the active dendritic membranes modifies the synchronizing properties of a pair of IF neurons with weak symmetric coupling. That is, we calculate $\text{sign}(K_{T_0}^l(0))$ using Eqs. (9) to (11) and Appendix A. The results are displayed in Fig. 5B for $r_l = 0.1 \Omega\text{m}^2$ (with $\omega_{\max} \approx 1.4 \tau_d^{-1}$) and in Fig. 5C for

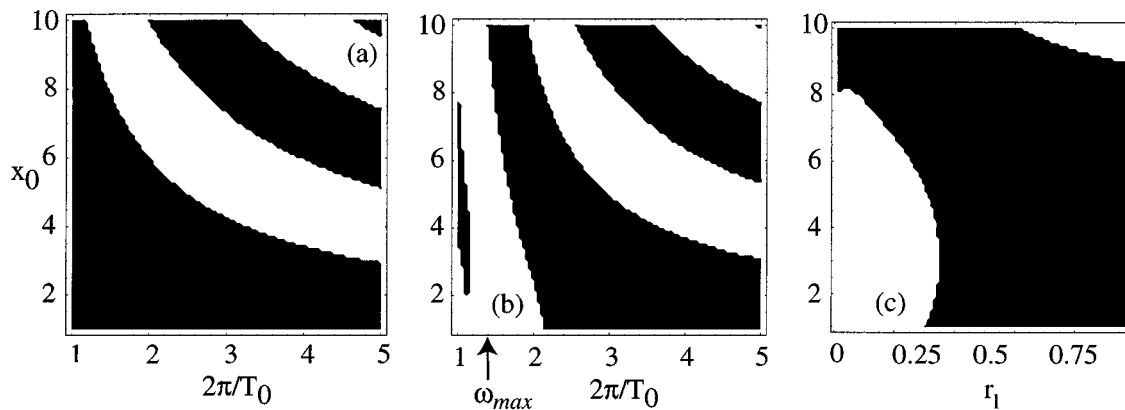


Figure 5. Illustration of resonantlike synchronization in the presence of active dendrites. Stability regions for the synchronous state in the weak coupling regime are plotted as a function of dendritic distance x_0 (in units of σ). White (black) stripes denote stability (instability) for excitatory coupling. A: Variable collective frequency $2\pi/T_0$ (in units of τ_d^{-1}) and infinite inductive resistance (passive membranes). B: Variable collective frequency $2\pi/T_0$ (in units of τ_d^{-1}) and fixed inductive resistance $r_l = 0.1 \Omega\text{m}^2$ (resonant membranes). C: Variable inductive resistance r_l (in units of Ωm^2) and fixed collective frequency $2\pi/T_0 = 1.5 \tau_d^{-1}$. Other membrane parameters are as in Fig. 4.

$2\pi/T_0 = 1.5 \tau_d^{-1}$. Comparison with the nonresonant case, Fig. 5A, shows that around the resonant frequency ω_{\max} there is a greatly enhanced region in parameter space in which the synchronous state is stable (unstable) for excitatory (inhibitory) coupling.

4. Bursting in the Strong Coupling Regime

In a recent study of a pair of pulse-coupled IF neurons with synaptic (α -function) and discrete axonal delays, we have shown analytically that Eq. (13) is necessary but not sufficient to guarantee stability of a phase-locked state in the strong coupling regime (Bressloff and Coombes, 1998a, 1998b). For example, a pair of IF neurons can desynchronize to a state in which one neuron becomes quiescent (oscillator death). We analyzed such spike train transitions by considering perturbations of the firing times and carrying out a linear stability analysis along analogous lines to van Vreeswijk (1996) and Gerstner et al. (1996). We established that a fundamental mechanism for destabilization of a phase-locked state is the occurrence of a Hopf bifurcation in the firing times (see Bressloff and Coombes, (1998a, 1998b), for further details). It is interesting to note that the breakdown of 1 : 1 mode-locking leading to oscillator death has been observed in numerical simulations of two coupled Hodgkin-Huxley neurons (White et al., 1998). A condition for oscillator death in a pair of inhibitory IF neurons has also been derived by Chow (1998).

Spike train transitions from a 1 : 1 mode-locked state are also observed in the case of passive dendritic interactions. Direct numerical solution of the dynamics in the case of passive dendrites and inhibitory coupling can lead to oscillator death whereas for excitatory coupling phase-locking persists into the strong coupling regime. However, the picture is drastically altered for active membranes. This is illustrated in Fig. 6 where we display the results of direct simulations of a pair of IF neurons with excitatory coupling. The dendritic cable is represented by a coupled system of $N = 100$ electrical compartments labeled by $m = 0, \dots, N - 1$. We take zero flux boundary conditions at $m = 0, N - 1$. (See Appendix B for details). In the case of active dendrites ($r_l = 0.1 \Omega m^2$) a periodic bursting pattern is clearly seen with the spike trains of the two neurons synchronized. Similarly, a pair of inhibitory neurons can exhibit bursting patterns in which the activity of the two neurons alternates (see Fig. 7A). One also finds multistability in which bursting states co-exist

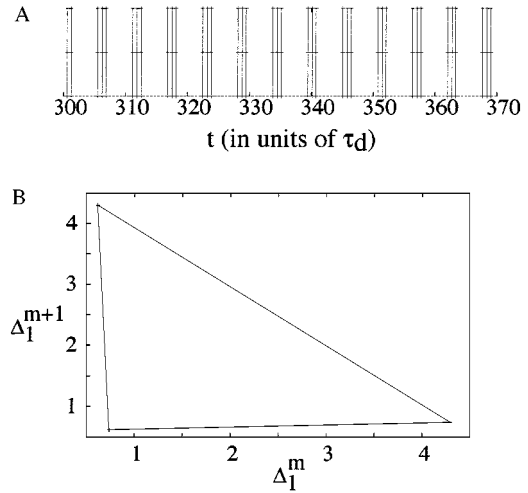


Figure 6. A: Direct numerical simulation of a pair of excitatory IF neurons with resonant ($r_l = 0.1 \Omega m^2$) dendritic membranes. Other membrane parameters are as in Fig. 4. Also $\epsilon = 20$, $T_0 = 2\pi$, and $x_0 = 2$. The dendritic cable is modeled in terms of $N = 100$ coupled electrical compartments (see Appendix B). The firing times of the two oscillators are represented with lines of different heights (marked with a + and a solid rectangle respectively). B: Periodic orbit of the ISIs of one of the neurons whose bursting pattern is displayed in Fig. 7B. The orbit is of period 3 with $\Delta_1^{m+3} = \Delta_1^m$ for all integers m .

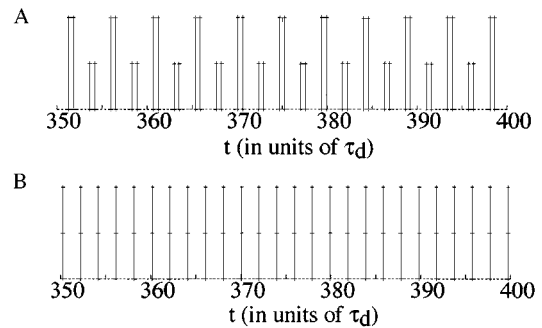


Figure 7. Direct numerical simulation of a pair of inhibitory IF neurons with resonant ($r_l = 0.1 \Omega m^2$) dendritic membranes, illustrating multistability. Other membrane parameters are as in Fig. 4. Also $\epsilon = -10$, $T_0 = 4\pi/3$ and $x_0 = 1$. The dendritic cable is modeled in terms of $N = 100$ coupled electrical compartments (see Appendix B). The firing times of the two oscillators are represented with lines of different heights (marked with a + and a solid rectangle respectively). A: Antisynchronous bursting state. B: Synchronous regular oscillations.

with regular periodic spike trains (Fig. 7B). Note that the potential role of active dendrites in the generation of a variety of neuronal firing patterns has recently been highlighted by Mainen and Sejnowski in their numerical study of a compartmental model of a neocortical

neuron with passive and active dendritic membranes (1996).

Although destabilization of phase-locked states in the strong coupling regime can be analyzed in terms of perturbations of the firing times, this approach does not help us determine the nature of the state that the system bifurcates to. We have recently established elsewhere that for synaptic and axonal delays, the qualitative dynamics of IF neurons with strong coupling can be understood by considering an analog or rate-coded version of the IF model (Bressloff and Coombes, 1998a, 1998b). In certain parameter regimes, it is also possible to obtain good quantitative agreement between the firing-rates of the analog model and the (time-averaged) spike trains of the IF model. However, this requires that the effective width of the underlying delay kernel $J(t)$ is not too small otherwise the neuron samples incoming spike trains sparsely (Bressloff and Coombes, 1998a, 1998b). We do not dwell on this particular issue here and focus on qualitative features of the dynamics reproduced by the analog model.

In the case of delays arising from dendritic structure, a rate-coded model can be obtained by reinterpreting $E_j(t)$ in Eq. (3) as a short-term average firing rate. That is, we define $X_i(t) = V_i(0, t)$ and take $E_j(t) = f(X_j(t))$ where $f(X)$ is the firing rate function

$$f(X) = \begin{cases} \left(T_{\text{ref}} + \ln \left[\frac{I + X}{I + X - 1} \right] \right)^{-1} & X > 1 - I \\ 0 & X < 1 - I. \end{cases} \quad (18)$$

A refractory period T_{ref} is introduced to ensure that the firing rate is bounded from above by T_{ref}^{-1} . Such an effect can be mimicked in the IF model by introducing inhibitory self-interactions (Gerstner, 1995). For the sake of clarity, we shall ignore the effects of refractory period in this article and set $T_{\text{ref}} = 0$. The basic conclusions of the article are unchanged if a refractory period is included. Under this approximation the integral Eq. (3) becomes

$$X_i(t) = \epsilon \int_{-\infty}^{\infty} G(x_0, t') \hat{f}(X_j(t - t')) dt', \quad (19)$$

with $j \neq i$ and where $G(x, t)$ is the Green's function of the passive or linearized, active cable. For convenience, we have introduced a bias term into Eq. (19) such that $f(X)$ is replaced by $\hat{f}(X) = f(X) - f(0)$. This ensures that $X_j = 0$ for all j is a fixed point of Eq. (19). In order to investigate the stability of the zero fixed point,

we linearize Eq. (19) and substitute $X_j(t) = e^{\lambda t} \bar{X}_j$ into the resulting linearized integral equation. This generates the following eigenvalue equation (after absorbing a factor of $f'(0)$ into the definition of ϵ):

$$\pm 1 = \epsilon \tilde{G}(x_0, -i\lambda) = \frac{\epsilon}{D} \frac{e^{-\gamma(-i\lambda)x_0}}{\gamma(-i\lambda)}, \quad (20)$$

where $\tilde{G}(x, \omega)$ is the transfer function of Eq. (11), and ± 1 corresponds to activation of the linear mode $(\bar{X}_1, \bar{X}_2) = (1, \pm 1)$. The fixed point will be stable if all solutions λ of Eq. (20) have negative real part. From the explicit form of $\gamma(\omega)$, Eqs. (14) to (16), and Appendix A, it can be shown that it is stable in the weak coupling regime for all x_0 . n.b. $|\tilde{G}(x_0, -i\lambda)|$ is bounded from above when $\text{Re } \lambda > 0$ so that for sufficiently small ϵ all solutions λ of Eq. (20) must have a negative real part.

As $|\epsilon|$ is increased from zero, an instability may occur in at least two distinct ways. If a single real eigenvalue λ crosses the origin in the complex λ -plane, then a static bifurcation can occur leading to the emergence of additional fixed point solutions, which correspond, say, to inhomogeneous firing rates. On the other hand, if a pair of complex conjugate eigenvalues $\lambda = \lambda_R \pm i\lambda_I$ crosses the imaginary axis ($\lambda_R = 0$) from left to right in the complex plane, then a Hopf bifurcation can occur leading to the formation of periodic solutions—that is, time-dependent firing rates. Therefore, in order to investigate the stability of the fixed point in the strong coupling regime, we substitute $\lambda = i\beta$ into Eq. (20) and equate real and imaginary parts to yield

$$\pm 1 = \frac{\epsilon}{D} \frac{e^{-a(\beta)x_0}}{a(\beta)^2 + b(\beta)^2} \quad (21a)$$

$$\times [a(\beta) \cos(b(\beta)x_0) - b(\beta) \sin(b(\beta)x_0)] \\ 0 = b(\beta) \cos(b(\beta)x_0) + a(\beta) \sin(b(\beta)x_0), \quad (21b)$$

where $a(\beta)$ and $b(\beta)$ denote the real and imaginary parts of $\gamma(\omega)$ (see Appendix A), and ± 1 again denotes excitation of the eigenmode $(1, \pm 1)$. One solution to equation (21b) is $\beta = 0$ (since $b(\beta) = 0$). Equation (21a) then shows that the eigenmode $(1, \pm 1)$ is excited at the critical coupling $\epsilon = \pm \epsilon_S$, with $\epsilon_S > 0$ and

$$1 = \frac{\epsilon_S}{D} \frac{e^{-a(0)x_0}}{a(0)}, \quad (22)$$

where $a(0) = \text{Re}\gamma(0) = \sqrt{(r + r_l)/r_l} \sigma^{-1}$. In the case of inhibitory coupling, activation of the mode $(1, -1)$

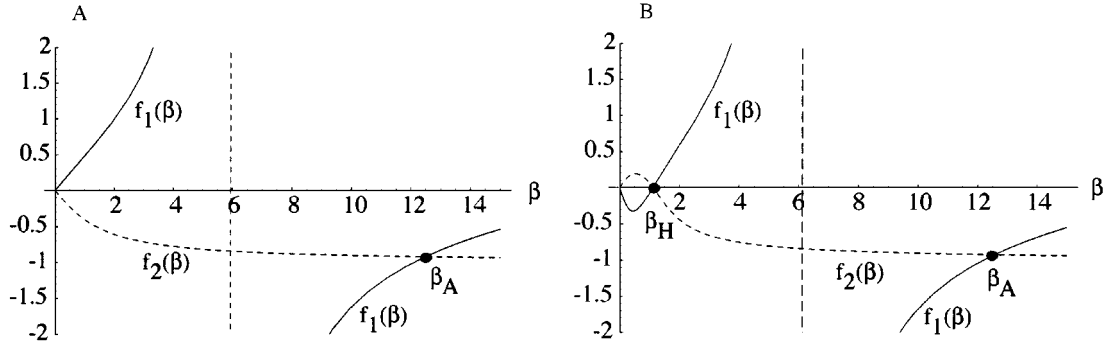


Figure 8. Solutions of Eq. (21b) for the analog model. Here $f_1(\beta) = \tan(b(\beta)x_0)$ and $f_2(\beta) = -b(\beta)/a(\beta)$ with $x_0 = 1$ (in units of σ). A: $r_l = 10 \Omega\text{m}^2$ (nonresonant), B: $r_l = 0.1 \Omega\text{m}^2$ (resonant). Other membrane parameters as in Fig. 4.

leads to a state in which one neuron is active and the other quiescent. Similarly, in the case of excitatory coupling the instability corresponds to the activation of the linear mode (1, 1), which indicates that the pair of analog neurons bifurcates to another homogeneous state rather than to one with an active/inactive pair. Such behavior is consistent with that found for a pair of IF oscillators with symmetric excitatory coupling.

In Fig. 8 we determine graphically nonzero solutions β of Eq. (21b) for both passive and active membranes by finding the intercepts of the functions $f_1(\beta) = \tan(b(\beta)x_0)$ and $f_2(\beta) = -b(\beta)/a(\beta)$. In the passive case (see Fig. 8A), the smallest nonzero solution is at $\beta = \beta_A$ with $\tanh(b(\beta_A)x_0) < 0$, $\pi/2 < b(\beta_A)x_0 < \pi$. It follows that the corresponding critical coupling is $\epsilon = \pm\epsilon_A$, $\epsilon_A > 0$, where \pm denotes excitation of the eigenmodes (1, ∓ 1) and

$$1 = -\frac{\epsilon_A e^{-a(\beta_A)x_0}}{D a(\beta_A)} \cos(b(\beta_A)x_0). \quad (23)$$

It turns out that $\epsilon_A \gg \epsilon_S$ so that, in practice, the fixed point destabilizes via the static bifurcation at $\epsilon = \pm\epsilon_S$. On the other hand, for active membranes exhibiting resonance it is possible for a dynamic instability to arise rather than a static one. This is true for the example shown in Fig. 8B, where an additional nonzero solution β_H of Eq. (21) emerges on the first branch of the function $\tanh(b(\beta)x_0)$ with $b(\beta_H) = 0$. This is a consequence of an additional zero for $b(\beta)$, see Fig. 11. The associated critical coupling is given by

$$1 = \frac{\epsilon_H e^{-a(\beta_H)x_0}}{D a(\beta_H)}. \quad (24)$$

In Fig. 9 we plot ϵ_H and ϵ_S as a function of r_l for $x_0 = 1$. It can be seen that there exists a critical inductive

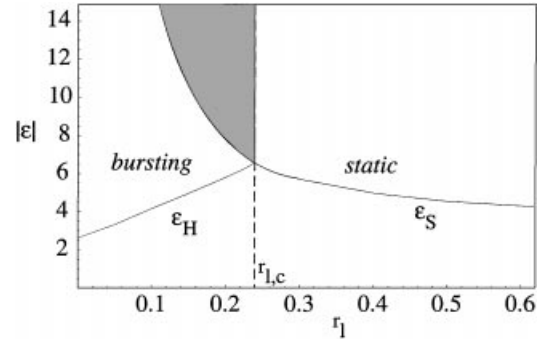


Figure 9. Critical couplings ϵ_S and ϵ_H for destabilization of a pair of analog neurons with symmetric coupling as a function of the inductive resistance r_l (in units of Ωm^2) with $x_0 = 1$ (in units of σ). Other membrane parameters are as in Fig. 4. There exists a critical inductive resistance $r_{l,c} \approx 0.24$ such that for $r_l < r_{l,c}$ a dynamic instability occurs leading to period firing-rates (bursting). On the other hand, states with constant firing-rates bifurcate when $r_l > r_{l,c}$ and, in the case of inhibitory coupling, one of the neurons ceases to fire (oscillator death). In the shaded region multistable solutions can occur.

resistance $r_{l,c} \approx 0.24$ beyond which a Hopf bifurcation cannot occur. That is, for $r > r_{l,c}$ a static bifurcation occurs at $|\epsilon| = \epsilon_S$ as described above. However, for $r < r_{l,c}$, the zero fixed point destabilizes when $|\epsilon| = \epsilon_H$ leading to a state with a time-periodic variation of the firing-rates. In the case of excitatory coupling the two neurons have the same firing-rate (due to activation of the linear mode (1, 1)) whereas the level of activity alternates between the pair in the case of inhibitory coupling (due to activation of the mode (1, -1)). These two cases are illustrated in Fig. 10. It is also possible for multistable solutions to occur when $\epsilon > \epsilon_S, \epsilon_H$ (shaded region in Fig. 9). For example, one finds that a stable limit cycle coexists with stable fixed points. This was also seen in the IF model (see Fig. 7B).

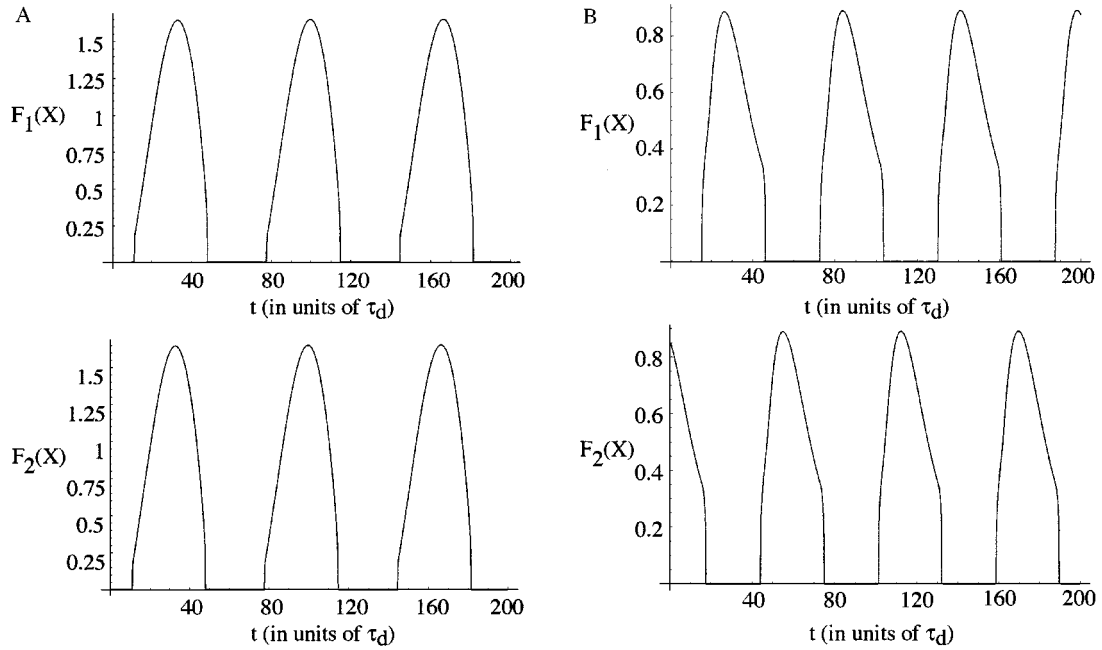


Figure 10. Direct numerical simulation of a pair of analog neurons with resonant ($r_l = 0.1 \Omega\text{m}^2$) dendritic membranes. Other membrane parameters are as in Fig. 4 and $x_0 = 1$. The dendritic cable is modeled in terms of $N = 100$ coupled electrical compartments as in Fig. 6. A: Excitatory coupling $\epsilon = 5$. The firing rates of both neurons are displayed and are seen to exhibit synchronized oscillations. B: Inhibitory coupling $\epsilon = -5$. The firing rates now exhibit antiphase oscillations.

5. Discussion

In this article we established analytically how active dendrites can have a major effect on the firing patterns of interacting neurons, even when the dendritic membranes are assumed to operate within a linear regime. This linear approximation allowed us to draw on a wide range of mathematical techniques including linear stability analysis, bifurcation theory, and Green's function methods. We first identified a form of resonantlike synchronization in which there is a strongly enhanced tendency to synchronize for weak excitatory coupling when the resonant frequency of the dendritic membrane approximately matches the collective frequency of the oscillators. We then showed how active dendrites can destabilize a pair of phase-locked neurons in the strong coupling regime leading to periodic bursting patterns and multistability. The basic idea that active dendrites can modulate a range of firing patterns is consistent with recent numerical work by Mainen and Sejnowski (1996) on compartmental models of neocortical neurons. They found that a wide variety of periodic and bursting firing patterns can be generated by appropriate choices of membrane parameters and dendritic

morphologies. Our work suggests that such complexity could arise, at least in part, from relatively straightforward processes.

Acknowledgments

I would like to thank Steve Coombes for helpful comments during the completion of this paper. The research was supported by grant number GR/K86220 from the EPSRC (UK).

Appendix A

We indicate how to calculate the function $h(\omega)$ defined by Eq. (10), which appears throughout our analysis of phase-locking in IF network dynamics. Using the fact that $K_T(\phi)$ is real, we rewrite the Fourier series (9) as

$$K_T(\phi) = \frac{1 - e^{-T}}{T} \sum_{m=-\infty}^{\infty} [h_R(\omega_m) \cos(2\pi m\phi) - h_I(\omega_m) \sin(2\pi m\phi)], \quad (\text{A1})$$

where $\omega_m = 2\pi m/T$ and $h_R(\omega)$ and $h_I(\omega)$ denote respectively the real and imaginary parts of the function $h(\omega)$. Taking the real and imaginary parts of Eq. (10) we obtain the pair of equations

$$h_R(\omega) = \frac{e^{-a(\omega)x_0}}{(1 + \omega^2)(a(\omega)^2 + b(\omega)^2)} \times (\cos(b(\omega)x_0)[a(\omega) - \omega b(\omega)] - \sin(b(\omega)x_0)[b(\omega) + \omega a(\omega)]) \quad (\text{A2})$$

$$h_I(\omega) = -\frac{e^{-a(\omega)x_0}}{(1 + \omega^2)(a(\omega)^2 + b(\omega)^2)} \times (\sin(b(\omega)x_0)[a(\omega) - \omega b(\omega)] + \cos(b(\omega)x_0)[b(\omega) + \omega a(\omega)]), \quad (\text{A3})$$

where we have used the decomposition $\gamma(\omega) = a(\omega) + ib(\omega)$. Note that $h_R(-\omega) = h_R(\omega)$ and $h_I(-\omega) = -h_I(\omega)$.

The real functions $a(\omega)$, $b(\omega)$ are determined by the membrane impedance $z_m(\omega)$ of Eq. (14). In the case of passive dendrites, we find from Eqs. (14) and (15) that

$$a(\omega) = \frac{1}{\sigma} \sqrt{\frac{1}{2} [1 + \sqrt{1 + (\tau_d \omega)^2}]}, \quad (\text{A4})$$

$$b(\omega) = \frac{\text{sign}(\omega)}{\sigma} \sqrt{\frac{1}{2} [-1 + \sqrt{1 + (\tau_d \omega)^2}]}, \quad (\text{A5})$$

where $\sigma = \sqrt{D\tau_d}$ is the membrane space constant. The analysis is slightly more involved for active dendrites where $z_m(\omega)$ is given by Eq. (16). First, we decompose $z_m(\omega)$ into real and imaginary parts, $z_m(\omega) = r[u(\omega) + iv(\omega)]$, where

$$u(\omega) = \frac{r_l[r + r_l - l\tau_d\omega^2] + l\omega^2[l + r_l\tau_d]}{A\omega^4 + B\omega^2 + C} \quad (\text{A6})$$

$$v(\omega) = \frac{l\omega[r + r_l - l\tau_d\omega^2] - r_l\omega[l + r_l\tau_d]}{A\omega^4 + B\omega^2 + C}, \quad (\text{A7})$$

and $A = (\tau_d l)^2$, $B = l^2 + (\tau_d r_l)^2 - 2\tau_d r l$, $C = (r + r_l)^2$. Note that $u(\omega)$, $v(\omega)$ are both dimensionless. Similarly, writing $\gamma(\omega) = a(\omega) + ib(\omega)$, we obtain the following result from Eq. (14):

$$a(\omega) = \frac{1}{\sigma} \sqrt{\frac{u(\omega) + \sqrt{u(\omega)^2 + v(\omega)^2}}{2[u(\omega)^2 + v(\omega)^2]}} \quad (\text{A8})$$

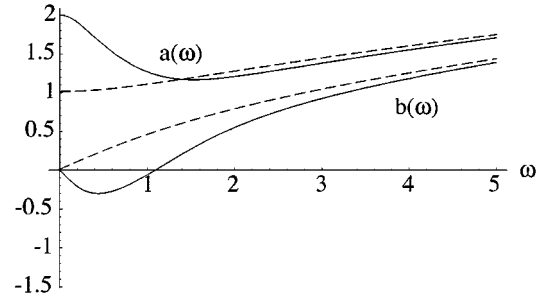


Figure 11. Real and imaginary parts $a(\omega)$, $b(\omega)$ of $\gamma(\omega)$ for non-resonant (dashed curves) and resonant (solid curves) dendritic membranes.

$$b(\omega) = -\frac{\text{sign}(v(\omega))}{\sigma} \times \sqrt{\frac{-u(\omega) + \sqrt{u(\omega)^2 + v(\omega)^2}}{2[u(\omega)^2 + v(\omega)^2]}}. \quad (\text{A9})$$

The functions $a(\omega)$ and $b(\omega)$ are plotted in Fig. 11 for both resonant and nonresonant cases. Note the existence of an additional zero for $b(\omega)$.

Appendix B

In the presence of active linearized membranes the cable Eq. (2) is replaced by the pair of equations

$$\frac{\partial V_i(x, t)}{\partial t} = -\frac{V_i(x, t)}{\tau_d} + D \frac{\partial^2 V_i(x, t)}{\partial x^2} - \frac{I_i(x, t)}{c} + \epsilon P(x) E_j(t) \quad (\text{B1})$$

$$l \frac{\partial I_i(x, t)}{\partial t} = -r_l I_i(x, t) + V_i(x, t), \quad (\text{B2})$$

with $I_i(x, t)$ the current through the inductive branch of the equivalent circuit shown in Fig. 3B. In the compartmental model version of these equations used in our direct simulations (see Section 4), we discretize the above cable equation using a finite-difference approximation scheme. The cable is then represented by a system of N coupled electrical compartments of length Δs labeled by $m = 0, \dots, N - 1$ (see Fig. 3). Denoting a single time step by Δt , we ensure that the condition $\Delta t / (\Delta s)^2 < 1/2$ is satisfied so that the finite-difference scheme is convergent. In practice, we take $\Delta t = 0.001$ and $\Delta s = 0.2$. The compartmentalized cable equation

takes the explicit form (after setting $\tau_d = D = 1$)

$$\begin{aligned} \frac{V_{i,m}(t + \Delta t) - V_{i,m}(t)}{\Delta t} &= -V_{i,m}(t) \\ &+ \frac{1}{(\Delta s)^2} [V_{i,m+1}(t) + V_{i,m-1}(t) - 2V_{i,m}(t)] \\ &- \frac{I_{i,m}(t)}{c} + \frac{\epsilon}{\Delta s \Delta t} \delta_{m,p} \delta_j(t), \quad j \neq i \end{aligned} \quad (\text{B3})$$

$$I_{i,m}(t + \Delta t) - I_{i,m}(t) = V_{i,m}(t) - r_l I_{i,m}(t) \quad (\text{B4})$$

for $j = 1, 2$. Here $\delta_j(t) = 1$ if oscillator j is at threshold at time t and is zero otherwise (i.e., $\delta_j(t)/\Delta t$ is a discrete approximation of the term $E_k(t)$). Similarly, $\delta_{p,m} = 1$ if $m = p$ and is zero otherwise, where p labels the compartment stimulated by the input (that is, $\delta_{p,m}/\Delta s$ is a discrete approximation of $P(x) = \delta(x - x_0)$). We take zero flux boundary conditions at $m = 0, N - 1$.

References

- Abbott LF, Farhi E, Gutmann S (1991) The path integral for dendritic trees. *Biol. Cybern.* 66:61–70.
- Abbott LF, Kepler TB (1991) Model neurons: From Hodgkin-Huxley to Hopfield. In: L Garrido, ed. *Statistical Mechanics of Neural Networks. Lecture Notes in Physics* 368:5–18.
- Amitai Y, Friedman A, Connors BW, Gutnick MJ (1993) Regenerative activity in the apical dendrites of pyramidal cells in neocortex. *Cereb. Cortex* 3:26–38.
- Bressloff PC (1994) Dynamics of compartmental model recurrent neural networks. *Phys. Rev. E* 50:2308–2319.
- Bressloff PC (1995) Dynamics of a compartmental model integrate-and-fire neuron with somatic potential reset. *Physica D* 80:399–412.
- Bressloff PC, Coombes S (1997) Physics of the extended neuron. *Int. J. Mod. Phys.* 11:2343–2392.
- Bressloff PC, Coombes S (1998a). Desynchronization, mode-locking and bursting in strongly coupled integrate-and-fire oscillators. *Phys. Rev. Lett.* 81:2168–2171.
- Bressloff PC, Coombes S (1998b) Dynamics of strongly coupled spiking neurons. *Neural Comput.*, in press.
- Bressloff PC, de Souza B (1998) Neural pattern formation in networks with dendritic structure. *Physica D* 115:124–144.
- Chow CC (1998) Phase-locking in weakly heterogeneous neuronal networks. *Physica D* 118:343–370.
- Coss RG, Perkel DH (1985) The function of dendritic spines: A review of theoretical issues. *Behav. Neural. Biol.* 44:151–185.
- Crawford AC, Fettiplace R (1981) An electrical tuning mechanism in turtle cochlear hair cells. *J. Physiol.* 312:377–412.
- Crook SM, Ermentrout GB, Bower JM (1998) Dendritic and synaptic effects in systems of coupled cortical oscillators. *J. Comp. Neurosci.* 5:315–329.
- Crook SM, Ermentrout GB, Vanier M, Bower JM (1997) The role of axonal delay in the synchronization of networks of coupled cortical oscillators. *J. Comp. Neurosci.* 4:161–172.
- Gerstner W (1995) Time structure of the activity in neural-network models. *Phys. Rev. E* 51:738–758.
- Gerstner W, van Hemmen JL, Cowan JD (1996) What matters in neuronal locking. *Neural Comput.* 8:1689–1712.
- Jackson ME, Cauler LJ (1997) Evaluation of simplified compartmental models of reconstructed neocortical neurons for use in large-scale simulations of biological neural networks. *Brain Res. Bull.* 44:7–17.
- Jaeger D, De Schutter E, Bower JM (1997) The role of synaptic and voltage-gated currents in the control of Purkinje cell spiking: A modeling study. *J. Neurosci.* 17:91–106.
- Johnston D, Magee JC, Colbert CM, Christie BR (1996) Active properties of neuronal dendrites. *Annual Rev. Neurosci.* 19:165–186.
- Kistler WM, Gerstner W, van Hemmen JL (1997) Reduction of the Hodgkin-Huxley equations to a single-variable threshold model. *Neural Comput.* 9:1015–1045.
- Koch C (1984) Cable theory in neurons with active, linearized membranes. *Biol. Cybern.* 50:15–33.
- Koch C, Poggio T (1983) A theoretical analysis of electrical properties of spines. *Proc. Roy. Soc. Lond. B* 218:455–477.
- Mainen ZF, Sejnowski TJ (1996) Influence of dendritic structure on firing pattern in model neocortical neurons. *Nature* 382:363–366.
- Mel BW (1994) Information processing in dendritic trees. *Neuro. Comput.* 6:1031–1085.
- Miller JP, Rall W, Rinzel J (1985) Synaptic amplification by active membrane in dendritic spines. *Brain Res.* 325:325–330.
- Perkel DH, Mulloney B, Budelli RW (1981) Quantitative methods for predicting neuronal behaviour. *Neurosci.* 6:823–837.
- Poggio T, Torre V (1977) A new approach to synaptic interactions. *Lecture notes in biomathematics* 21:89–115.
- Poolos NP, Kocsis JD (1990) Dendritic action potentials activated by NMDA receptor-mediated EPSPs in CA1 hippocampal pyramidal cells. *Brain Res.* 524:342–346.
- Qian N, Sejnowski TJ (1989) An electro-diffusion model for computing membrane potentials and ionic concentrations in branching dendrites, spines and axons. *Biol. Cybern.* 62:1–15.
- Rall W (1962) Theory of physiological properties of dendrites. *Ann. N.Y. Acad. Sci.* 96:1071–1092.
- Rall W (1964) Theoretical significance of dendritic trees for neuronal input-output relations. In: R Reiss, ed. *Neural Theory and Modelling*. Stanford University Press, Stanford.
- Rall W (1989) Cable theory for dendritic neurons. In: C Koch, I Segev, eds. *Methods of Neuronal Modeling: From Synapses to Networks*, MIT Press, Cambridge, MA, pp. 9–62.
- Segev I, Fleshman JW, Burke RE (1989) Compartmental models of complex neurons. In: C Koch, I Segev, eds. *Methods of Neuronal Modeling: From Synapses to Networks*. MIT Press, Cambridge, MA, pp. 63–96.
- Shepherd GM, Brayton RK (1987) Logic operations are properties of computer-simulated interactions between excitable dendritic spines. *Neuroscience* 21:15–166.
- Stuart G, Sakmann B (1994) Active propagation of somatic action potentials into neocortical pyramidal cell dendrites. *Nature Lond.* 367:69–72.
- Svoboda K, Denk W, Kleinfeld D, Tank DW (1997) In vivo dendritic calcium dynamics in neocortical pyramidal neurons dendrites. *Nature Lond.* 385:161–165.

- Torre V, Owen WG (1983) High-pass filtering of small signals by the rod network in the retina of the toad *Bufo Marinus*. *J. Biophys.* 41:305–324.
- Tuckwell HC (1988) Introduction to Theoretical Neurobiology. Cambridge University Press, Cambridge, MA, Vol. 1.
- van Vreeswijk C (1996) Partial synchronization in populations of pulse-coupled oscillators. *Phys. Rev. E.* 54:5522–5537.
- van Vreeswijk C, Abbott LF, Ermentrout GB (1994) When inhibition not excitation synchronizes neural firing. *J. Comp. Neurosci.* 1:313–321.
- White JA, Chow CC, Ritt J, Soto-Trevino C, Kopell N (1998) Synchronization and oscillatory dynamics in heterogeneous, mutually inhibited neurons. *J. Comput. Neurosci.* 5:5–16.
- Wong RK, Prince DA, Basbaum AI (1979) Intradendritic recordings from hippocampal neurons. *Proc. Natl. Acad. Sci. USA* 76:986–990.
- Zador A, Koch C, Brown TH (1990) Biophysical model of a Hebbian synapse. *Proc. Natl. Acad. Sci. USA* 87:6718–6722.